Surface & Coatings Technology 502 (2025) 131942

Contents lists available at ScienceDirect

Surface & Coatings Technology

journal homepage: www.elsevier.com/locate/surfcoat

Design of DC semi-industrial magnetron-sputtered W-Ti-N/Ag composite films: Insights into the microstructure and mechanical properties

Jing Luan [b,c], Yiping Wang [a], Songtao Dong [a], Manuel Evaristo [b,c], Filipe Fernandes [b,c,d], Albano Cavaleiro [b,c,e], Hongbo Ju [a,b,c,e,*]

[a] Jiangsu University of Science and Technology, School of Materials Science and Engineering, Mengxi Road 2, Zhenjiang, Jiangsu Province 212003, China
[b] University of Coimbra, CEMMPRE-Centre for Mechanical Engineering Materials and Processes, Department of Mechanical Engineering, Rua Luís Reis Santos, Coimbra 3030-788, Portugal
[c] University of Coimbra, ARISE, Department of Mechanical Engineering, Rua Luís Reis Santos, 3030-788 Coimbra, Portugal
[d] CIDEM, ISEP - Polytechnic of Porto, Rua Dr. António Bernardino de Almeida, 4249-015 Porto, Portugal
[e] University of Ljubljana, Faculty of Mechanical Engineering, TINT - Laboratory for Tribology and Interface Nanotechnology, Aškerčeva 6, 1000 Ljubljana, Slovenia

ARTICLE INFO

Keywords:
DC magnetron sputtering system
W-Ti-N/Ag composite films
Microstructure
Mechanical properties

ABSTRACT

A semi-industrial magnetron sputtering system was employed to deposit a series of W-Ti-N/Ag composite films with varying Ag content, aiming to provide practical parameters for industrial-scale PVD applications. The films were deposited by DC sputtering a W + 30 wt%Ti alloy target and an Ag target in an Ar and N_2 atmosphere. The results indicated that the composite films, regardless of Ag content, exhibited a face-centered cubic (fcc) structure and consisted of a three-phase mixture of W_2N, TiN and Ag. The Ag particles were embedded within the crystalline grains of solid solution of $(WTi)_2N$ and (TiW)N, resulting in grain refinement and increased interface density in the films. The predominant cross-section fracture of the Ag-alloyed was identified as transgranular. Both hardness and elastic modulus of the composite films gradually decreased with the Ag content due to the soft nature of the Ag phase.

1. Introduction

As modern industry continues to evolve, the challenges of energy consumption and resource wastage caused by wear have become increasingly severe, posing significant obstacles to global efforts toward green and sustainable development [1,2]. Lubrication is essential in minimizing friction and wear; however, conventional lubricants such as oil and grease are not only environmentally detrimental but also restricted in their temperature range, rendering them insufficient to meet the growing demand for eco-friendly, wide-temperature lubrication solutions [3,4]. Over the past two decades, the development of efficient solid lubricating film materials for harsh service environments based on the concept of adaptation to meet the increasingly diverse and multi-condition green lubrication needs has been a hot and cutting-edge topic in the field of surface engineering [5].

Due to their exceptional hardness and wear resistance, transition metal or its nitride films have been extensively studied and have been industrially applied in fields such as cutting tools and molds [6,7]. Tungsten was reported as one of the most representative candidates for the protective hard application, with the amazing melting point of around 3422 °C [8] and excellent hardness of about 25 GPa for the W nano-structured film [9]. Therefore, combination with other nonmetal elements, such as N, C and B, for synthesizing the W—N [10], or W—C [11], or W—B [12] composite film using the processes of RF/DC sputtering [13–17] or CVD [18], was considered as the effective method to enhance the mechanical and tribological properties [19]. The phase structure of the composite film was significantly influenced by the nonmetal element content in the films [20]. For instance, the phase of the WN_x films was changed from bcc-W for the N content below 9 at.%, to a mixture phases of bcc-W with fcc-W_2N for the N content in the range of 12–15 at.%, then to a single fcc-W_2N for the N content ranging from 30 to 50 at.%, finally to hcp-WN with a N content above 55 at.% [21]. Among these materials, nitride films such as W_2N hold significant potential for high-temperature self-lubricating applications due to their ability to in-situ generate Magnéli phases with a layered structure during high-temperature friction [22]. As a result, they have attracted

* Corresponding author at: Jiangsu University of Science and Technology, School of Materials Science and Engineering, Mengxi Road 2, Zhenjiang, Jiangsu Province 212003, China.
E-mail address: hbju@just.edu.cn (H. Ju).

https://doi.org/10.1016/j.surfcoat.2025.131942
Received 19 September 2024; Received in revised form 31 January 2025; Accepted 16 February 2025
Available online 17 February 2025

significant attention in the field of solid lubrication [23]. At present, the design and fabrication of composite (multilayer) films by incorporating additional elements, known as modulation layers, is a widely adopted strategy to enhance the overall performance of W_2N films. This method significantly enhances key properties such as mechanical strength, corrosion resistance, and wear resistance, effectively meeting the increasingly demanding requirements of advanced applications, including dry cutting and high-temperature lubrication [24]. For example, Beltrami et al. [25] successfully designed and prepared a CrN/W_2N multilayer film with excellent mechanical strength and corrosion resistance by alternating deposition of a corrosion-resistant CrN layer and a high-hardness W_2N layer. Braga et al. [26] compared the mechanical properties of W-Ti-N films on nitrided steel and non-nitrided steel and found that the introduction of Ti elements into the W_2N matrix can improve the hardness and corrosion resistance of the W_2(Ti)N film. Inspired by the "nc-TiN/a-SiN_x" model [27], our research team employed magnetron sputtering technology to introduce a controlled amount of Si into the W_2N matrix. This process leads to thermodynamic spinodal decomposition, resulting in a nanocomposite structure where W_2N nanocrystals are embedded within an amorphous Si_3N_4 atomic layer [28]. The mechanical properties of this type of film have been greatly improved [29]. Furthermore, we also prepared W-Ti-N films using W-20wt.%Ti composite targets by magnetron sputtering technology. The results show that the film hardness can reach up to 50 GPa [30]. Additionally, Ag is often added to hard nitride films as a lubricant agent to achieve wide temperature self-lubricating properties [31–37]. This type of nitride-based film materials containing Ag have been widely studied, for instance, TiN-Ag [38], NbN-Ag [39], VN-Ag [40], etc. What's more, the addition of a small amount of Ag to the nitride matrix can also enhance the mechanical properties to a certain extent, due to the combined effects of grain refinement and coherent strengthening [41].

Building on the current research, the addition of Ag to W-Ti-N thin films is anticipated to further enhance their mechanical properties. However, there have been relatively few studies focused on this specific combination. In addition, most research on Ag-containing nitride thin films utilizes small-sized targets in laboratory settings. To progress toward industrial applications, this study employs rectangular targets that closely resemble those used in industrial-scale equipment, along with semi-industrial magnetron sputtering technology, to fabricate W-Ti-N/Ag composite films. This study investigates the effect of Ag content on the microstructure and mechanical properties of the films, aiming to bridge the gap between laboratory research and practical, large-scale production.

2. Film deposition and measurements

The W-Ti-N/Ag composite films without and with Ag addition was deposited in a semi-industrial magnetron sputtering system (Teer Coatings Ltd., UK). Four cathodes connected with separated DC power supplies were evenly distributed in relation to the center of the chamber. Four targets with a purity of 99.9 % were mounted on the cathodes: two Ti target in the cathodes facing each other, and one Ag target facing one W + 30 wt% Ti alloy target. The size of each of the targets was 380 × 175 × 10 mm and the distance between the targets and the substrate was 150 mm. Silicon wafers were used as substrates, and were ultrasonically cleaned in acetone and ethanol for 15 min respectively. Then the cleaned substrates were put onto the substrate holder facing the targets. The schematic diagram of the deposition system is shown in Fig. 1. The substrates were etched in Ar^+ ions bombardment for 20 min under pulsed bias of 270 V at 0.5 Pa; the basic pressure was below 9 × 10–5 Pa. Then, the targets were cleaned under Ar (50 sccm), with a power of 1000 W, for 10 min to remove the contaminants on the target surface. After that, a pure Ti interlayer (1000 W for both Ti targets for 10 min) was deposited on the substrates by moving the shutter in the front of Ag and W + Ti alloy targets. Subsequently, a gradient interlayer was

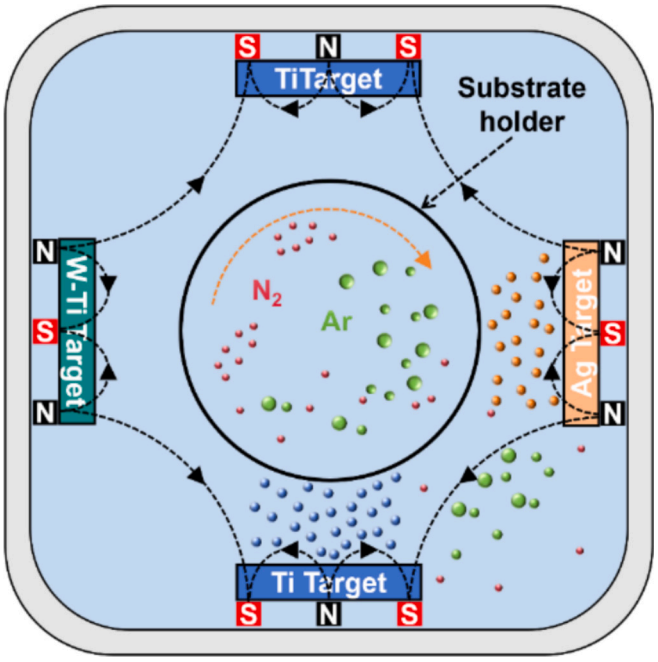

Fig. 1. Schematic diagram of semi-industrial magnetron sputtering system.

deposited by moving the shutter in the front of W + Ti alloy target (the power was increased from 0 to 1000 W) for 5 min. Following this, nitrogen gas was introduced into the chamber at a flow rate of 8 sccm, the shutter was moved in the front of both Ti targets. The W-Ti-N/Ag composite films with varying Ag content were deposited by fixing the W + Ti alloy target power at 2000 W, and adjusting the Ag target power for 0, 150, 175, 250, 350, and 450 W, respectively. During the deposition, a pulsed bias was kept at the substrate holder at −70 V (with the current of 0.15 A, power of 11 W, reverse times of 0.5vs, and frequency of 250 kHz), the substrate rotation speed was 10 rpm, the deposition time was set at 60 min, and no substrate heating was intentionally applied.

The elemental composition and the cross-section morphology of the films were characterized by Scanning Electron Microscope (SEM, ZEISS Merlin Gemini2) and its corresponding Energy Dispersive Spectrometer (EDS, Oxford, INCA Energy) system. The film's phase structure was characterized by X-Ray Diffraction (XRD) using a PANalytical X'Pert Pro diffractometer working in conventional mode. The main parameters used were as follows: (1) Cu Kα is the X-ray source, and the passing energy is 160 eV; (2) The 2θ angle range is 30–80°, and the scanning speed is 1°/min. An X-ray photoelectron spectrometer (XPS, ESCALAB250XI, Thermo Fisher, USA) was used to characterize the chemical bonds of the film, and the C 1 s peak at 284.8 eV was used as the reference peak to correct the XPS spectrum. Before characterization, the sample was etched to remove the influence of surface oxidation on the test results. The contaminants of the sample surface were removed using a gentle Ar^+ beam, sputtering at a primary energy of 800 eV at an angle of ~70° from the surface normal, held for 5 min, after the base pressure was below 2 × 10^{-7} Pa. The fitting of spectra was performed using the XPS CASA software, in which an adjustment of the peaks was performed using peak fitting with Gaussian–Lorentzian peak shape and Shirley type background subtraction. The cross-sectional microstructure of the composite film with different Ag content was investigate through a transmission electron microscope (TEM, Tecnai G2 F20, FEI, USA), with an acceleration voltage of 200 kV. The preparation of the TEM specimen can be carried out following these steps: (i) the specimen on the substrate of silicon wafer was cut and glued each other on the side of the films; (ii) the glued sample was polished on both sides using diamond sandpaper to decrease the thickness to ~0.1 mm; (iii) then, the sample was further polished to meet the requirement of measurement using the

Ion Beam Thinner system (GATAN 691, GATAN, USA) after attaching a molybdenum ring on the surface of the sample. The film thickness and film curvature radii were measured using the profilometer (DEKTAK-XT, Bruker, Germany), and then the residual stress of the films with different titanium content was calculated based on the Stoney's Eq. [42]. A nanoindentation tester (Micromaterials nano test Plataforma 1, UK) equipped with a diamond Berkovich indenter was used to characterize the film hardness and elastic modulus. The specific parameters were as follows: (1) Maximum loading force was 5 mN; (2) Holding time was 10 s; (3) Loading and unloading speed was 0.1 mN/s. To ensure the accuracy of the test data, 2 different areas were selected on the sample surface and 15 measurements were performed respectively, and the average value was taken.

3. Results and discussion

3.1. Elemental compositions and microstructure

Table 1 presents the EDS measured elemental compositions of the reference W-Ti-N film and the W-Ti-N/Ag composite films deposited at varying Ag target powers. The reference film contains approximately 46.3 at.% W, 24.9 at.% Ti, 27.4 at.% N, and 1.4 at.% O. The (W + Ti) to N ratio is around 2.6, indicating significant N vacancies, consistent with previous findings on magnetron-sputtered W-N-based films [43,44]. Additionally, the optimized W/Ti ratio of about 1.9 in this system has been shown to enhance toughness while maintaining high hardness [45].

As for the W-Ti-N/Ag composite films, the Ag content increases gradually with the rise in Ag target power but does so nonlinearly. There is a threshold between 175 and 250 W, beyond which Ag content increases significantly, indicating a more pronounced Ag deposition. This results in decreased W, Ti, and N content, while O content remains stable at around 2 at.%. The W/Ti and (W + Ti)/N ratios remain stable up to 175 W but decrease after surpassing 250 W, reflecting changes in film composition with higher Ag addition.

Fig. 2 shows the XRD spectra of the W-Ti-N reference film and the W-Ti-N/Ag composite films with different Ag contents. The figure also lists the positions of the standard peaks of fcc-W_2N, fcc-TiN and fcc—Ag, according to PDF-65-0715, 25–1257 and 65–2871 to analyze the film phase composition. As shown in this Fig., six diffraction peaks appear near 37°, 40°, 42°, 59°, 69°, and 73° in the XRD spectrum of the ternary W-Ti-N film, of which the diffraction peaks at 40° and 59° correspond to the transition layer Ti, and the diffraction peak near 69° comes from the silicon wafer substrate. In addition, the remaining three diffraction peaks are contributed by the crystal planes parallel to the sample surface in the deposited film, but the positions of the corresponding standard peaks of TiN and W_2N phases at the above three angles are very close. Therefore, it can be inferred from the spectrum that the W-Ti-N film exhibits a fcc structure, but it is difficult to determine the phase composition of the film. From the asymmetric shape of the diffraction peaks, it can be inferred that the three diffraction peaks can be split into two peaks, fcc-TiN and fcc-W_2N, so the film may be composed of two phases, fcc-TiN and fcc-W_2N. The XRD spectrum of the W-Ti-N/Ag composite film showed three diffraction peaks from the deposited film similar to the reference one. What's more, when the Ag content is higher than 26.7 at.%, the film shows a diffraction peak with very low intensity near 62°, which corresponds to the (222) crystal plane of fcc. Furthermore, compared with the W-Ti-N reference film, the diffraction peak of the W-Ti-N/Ag film gradually shifts to higher angles with the increase of Ag content, which may be related either to the formation of fcc-Ag phase in the films, or to the residual stresses.

Fig. 3 shows the XPS spectra of W-Ti-N/Ag films with different Ag contents, which are used to analyze the chemical bonding state of the films. Fig. 3(a) shows the full XPS spectra of films with Ag contents of 1.7 and 11.0 at.%, in which six different elements appear, namely W, Ti, Ag, N, O and C. C1s is the calibration peak [46], and the other elements are all from the deposited films, which is consistent with the characterization results in Table 1. Before the formal XPS characterization, although the sample was slightly etched to remove surface adsorption and oxide scale, the W and Ti sputtered out during the film deposition process may react with the residual oxygen and water vapor in the deposition chamber to produce a small amount of oxidized phase, resulting in the presence of O in the spectrum. Fig. 3(b) shows the W4f XPS spectrum of the film. There are three peaks in the spectrum, with the peak near 41.6 eV belongs to W 5p3/2 [47]. The remaining two peaks belonging to W4f can be split into four peaks. Among them, the two peaks at 35.6 and 37.8 eV have the highest intensity and belong to the W—N bond, for W_2N [48]; and the two peaks with lower intensity near 36.1 and 38.2 eV correspond to the W—O bond in WO_3 [49]. Fig. 3(c) is the XPS spectrum of Ti 2p. Two peaks appear in the spectrum, each of which can be split into three peaks, for a total of six. Among them, the peaks at 454.5 and 460.3 and the two peaks near 455.8 and 461.3 eV are Ti—N bonds in TiN [50]. The two peaks at 457.3 and 461.9 eV are Ti—O bonds in TiO_2 [51]. According to the two XPS peaks in the Ag 3d XPS spectrum shown in Fig. 3(d), it can be split into two peaks, which are Ag—Ag bonds near 368.1 and 374.1 eV respectively [52]. Fig. 3(e) shows the N 1 s spectrum. There is an XPS peak in the spectrum, which can be fitted into four peaks, namely: W—N bond at 397.3 eV [53], Ti—N bond at 397.8 eV [54], Ti-O-N bond at 399.2 eV [55], and satellite feature at 399.5 eV [56]. According to the integrated intensity shown in the figure, it can be seen that the main nitride phase in the film is W_2N. In addition, Fig. 3(f) shows O 1 s XPS spectra. An original peak appears in both spectra, which can be fitted into three peaks, namely Ti—O [57] at 529.9 eV, W—O [58] at 530.8 eV, and Ti-O-N [59] at 532.4 eV.

Fig. 4 shows the SEM images of the W-Ti-N film and the interface of the W-Ti-N/Ag film with different Ag contents. Regardless of the Ag content, the cross-section differentiates clearly the film, the interlayer and the substrate. GLAD morphological characteristic (glanding angle deposition) could be observed. The semi-industrial magnetron sputtering system was applied to deposit the film, and the substrate holder in the chamber was too big to parallel to the surface of the target and, thereby resulting in the gentle GLAD morphology of the film. As the Ag content increases, the thickness of the film gradually increases. Since the film is deposited by increasing the Ag target power for a constant deposition time, more Ag atoms are sputtered leading to thicker films. In addition, the Ag content also effects the cross-sectional characteristics of the film. In the cross-sectional image of the W-Ti-N reference film in Fig. 4 (a), a classical dense columnar structure can be observed, and

Table 1
Elemental compositions of W-Ti-N reference film, and W-Ti-N/Ag composite films with various Ag target powers.

Target Power of Ag(W)	Chemical composition (at.%)					W/Ti	(W + Ti)/N
	W	N	Ag	Ti	O		
0	46.6 ± 2.3	26.9 ± 1.3	0	25.1 ± 1.2	1.4 ± 0.1	1.9	2.7
150	45.9 ± 2.3	26.0 ± 1.3	1.7 ± 0.1	24.5 ± 1.2	1.9 ± 0.1	1.9	2.7
175	45.7 ± 2.3	25.0 ± 1.2	2.7 ± 0.1	24.9 ± 1.2	1.8 ± 0.1	1.8	2.8
250	39.3 ± 2.0	26.0 ± 1.3	11.0 ± 0.6	22.6 ± 1.1	1.7 ± 0.1	1.7	2.3
350	31.1 ± 1.6	22.6 ± 1.1	26.7 ± 1.3	18.4 ± 0.9	1.1 ± 0.1	1.7	2.2
450	28.6 ± 1.4	20.2 ± 1.0	32.6 ± 1.6	16.4 ± 0.8	2.3 ± 0.1	1.7	2.2

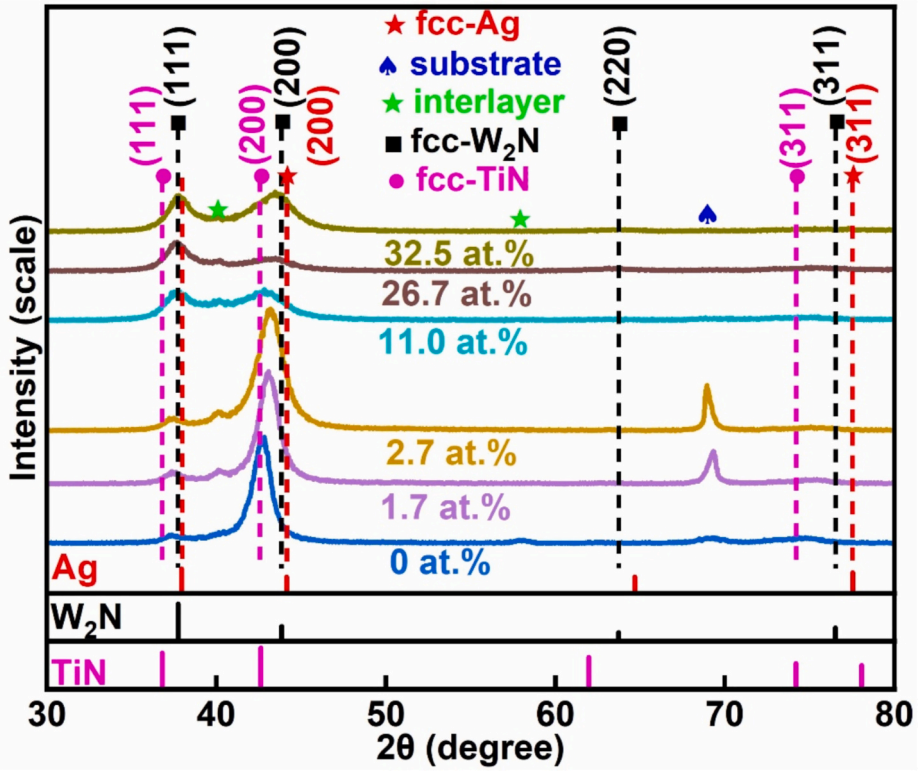

Fig. 2. XRD patterns of the reference W-Ti-N film and the W-Ti-N/Ag films with various Ag content.

most of the columnar crystals are about 200 nm wide. Two completely different zones, one smooth and another rough, can be observed (see detail in Fig. 4(a)). The proportion between both zones can be roughly calculated as half / half. The cross-sectional morphology of the film with an Ag content of 1.7 at.% is shown in Fig. 4(b). The film still presents a dense columnar crystal structure, but the width of the columnar crystal is significantly reduced compared to Fig. 4(a); its value is roughly within 50–100 nm. Although the refinement of the columns has significantly reduced compared to the reference one, the proportion of rough zones in the film cross-section has increased significantly; it is difficult to observe any smooth cross-section zone. When the Ag content in the film is 26.7 at.%, the cross-sectional characteristics of the film have changed significantly, and the results are shown in Fig. 4(c). The classic columnar crystal structure of the nitride ceramic film material completely disappears, the cross-section is rough.

To further investigate the effect of Ag on the evolution of film microstructure, cross-sectional TEM characterization was performed on W-Ti-N/Ag film samples with different Ag contents. Among them, the cross-sectional TEM results of the film with an Ag content of 1.7 at.% are shown in Fig. 5. The film shows a dense structure with some diffusely distributed darker zone (Fig. 5(a)). Based on previous TEM research results on nitride ceramic films containing soft metals, such as TiN/Ag, the darker zone may be attributed by the soft metal particles embedded in the nitride matrix [60]. To achieve this, selected area electron diffraction (SAED) was performed in both areas with (area I) and without (area II) black particles. Area I SAED is shown in Fig. 5(b), where the diffraction rings near the projection spot are the densest, indicating that the spacing between the crystal planes of the physical phases corresponding to the three diffraction patterns is very small. After calculation and comparison with PDF-65-0715, 25–1257 and 65–2871, the diffraction patterns correspond to the corresponding crystal planes of fcc-TiN, fcc-W_2N and fcc—Ag. The specific indexes are shown in the figure. This indicates that in region I, the film is fcc and three phases coexist. The SAED results of region II are shown in Fig. 5(c). Unlike region I, only two groups of diffraction patterns corresponding to fcc-TiN and fcc-W_2N appear in the spectrum at this time. This indicates that two phases co-exist in the film of region II. By comparing the SAED results of the two regions, it can be inferred that in region I, the particles with relatively high contrast are soft metal Ag, which is consistent with our previous TEM characterization structure. The HRTEM photograph of area I in Fig. 5(a) is shown in Fig. 5(d). Three groups of obvious lattice fringes appear in this HRTEM image, defined as I, II and III from top to bottom. The IFFT of the above three lattice fringes are shown in Fig. 5 (e), (f) and (g), respectively. According to the interplanar spacing, the corresponding crystal plane indices can be determined to be (111) and (200) crystal planes of fcc—Ag, fcc-TiN, and fcc-W_2N, respectively. It is important to note that the fcc-Ag in this HRTEM image is very large and no complete grain boundary can be observed in the field of view, which is inconsistent with the TiN/Ag composite film we reported previously [38].This is related to the semi-industrial magnetron equipment we used, because in this equipment, we placed a rectangular target of Ag and prepared the composite film by rotating the sample stage, instead of using a small laboratory target and confocal method to prepare the film as before. Unlike Fig. 5(d), only two different types of lattice fringes appeared in the HRTEM image from area II of Fig. 5(a), and their corresponding IFFTs are shown in Fig. 5(i) and (j) from top to bottom. According to the measured crystal plane spacing, the upper half of the HRTEM image belongs to fcc-W_2N (111), and the lower half belongs to fcc-TiN (111). No lattice fringes corresponding to fcc-Ag were observed, which is consistent with the result of Fig. 5(e).

In order to study the microstructural characteristics of the film with a higher Ag content, the cross section of the W-Ti-N/Ag film with an Ag content of 26.7 at.% was characterized by TEM, and the results are shown in Fig. 6. It can be observed from the TEM image of the film cross section given in Fig. 6(a) that the film presents a dense structure. A large number of black particles appear in the thin area of the film, which may belong to the soft metal Ag. In addition, the lower film thickness, in relation to that of Fig. 4, is due to the bombardment of Ar ions during the polishing of the sample using ion thinning system. The SAED spectrum of region I is shown in Fig. 6(b). Three groups of diffraction rings

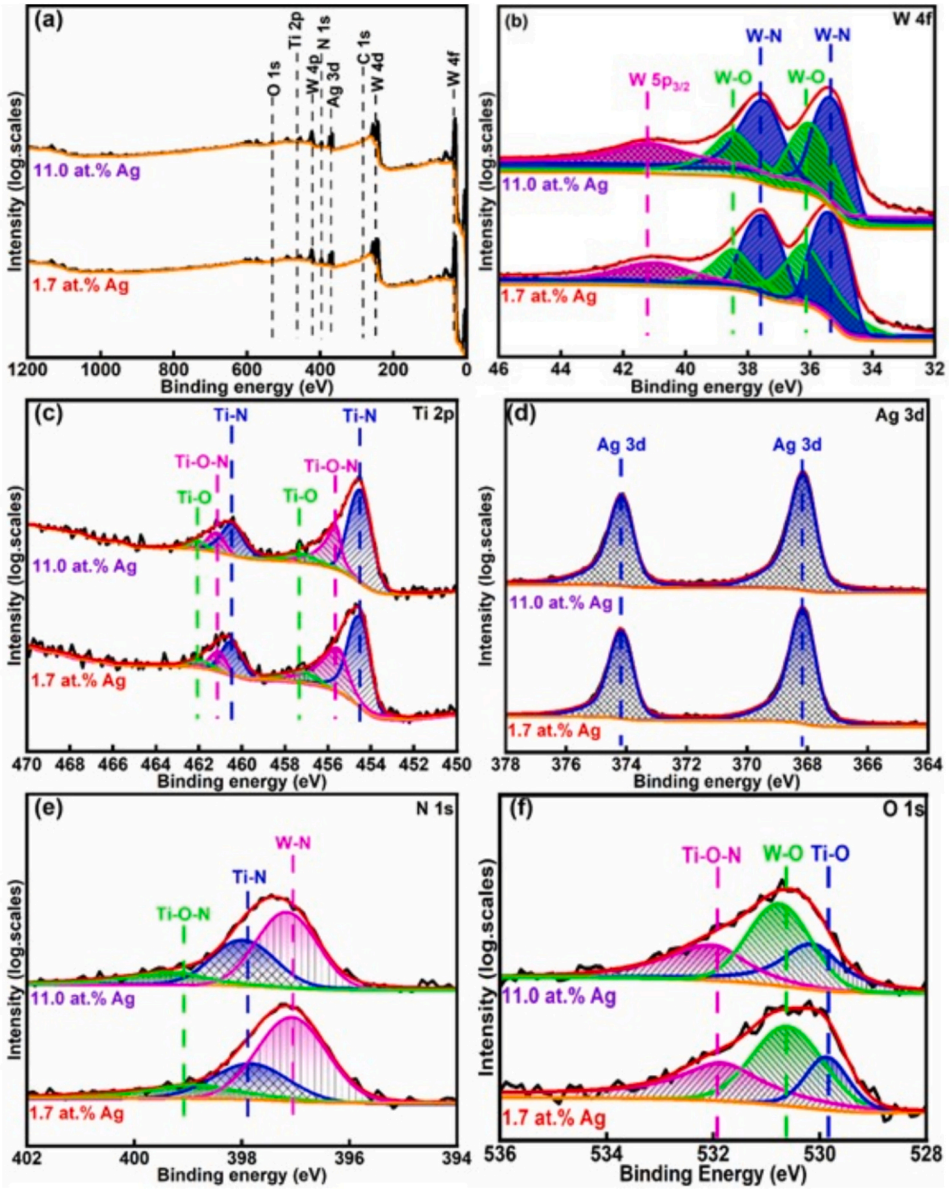

Fig. 3. Full-scanning XPS spectra (a), and the high-resolution ones of W 4f (b), Ti 2p (c), Ag 3d (d), N 1 s (e), and O 1 s (f), of the W-Ti-N/Ag films with various Ag content.

corresponding to different phases appear in the spectrum. For the diffraction ring closest to the projection spot, it come from fcc-TiN, due to tis largest value of plane spacing. The (111) and (200) crystal planes of the three phases of fcc-TiN, fcc-W_2N, and fcc-TiN are marked in the figure. The HRTEM image of the black particle in area I of Fig. 6(a) is shown in Fig. 6 (c) to confirm that the particle is Ag. According to the set of lattice fringes shown in Fig. 6(c), the interplanar spacing is 0.234 nm, corresponding to the fcc-Ag (111) crystal plane.

Studies of W-Ti-N films with varying Ti contents reveal that when the W/Ti ratio is below 4.2, the fcc-TiN phase forms, leading to the coexistence of two phases in the film: fcc-TiN and fcc-W_2N [61]. Therefore, the W-Ti-N reference film discussed in this paper is expected to exhibit a fcc structure with two coexisting phases: a solid solution of Ti in fcc-W_2N and a solid solution of W in fcc-TiN. Due to the close proximity of the standard peak positions for fcc-W_2N and fcc-TiN, the XRD spectrum of the reference sample displays three diffraction peaks at 37°, 43°, and 73°. However, the asymmetric shape of the diffraction peaks suggests that these peaks are composed of overlapping contributions from fcc-W_2N and fcc-TiN phases with the same crystal plane indices. This microstructural characteristic of the comparison sample is also confirmed by the HRTEM and SAED results presented in our previously published papers. It is widely accepted that the soft metal of Ag is difficult to dissolve in the nitride ceramic lattice [62]. Hence, even when the Ag content is extremely low, such as 1.7 at.%, the Ag—Ag bond corresponding to the Ag phase can be detected in the W-Ti-N/Ag film (XPS results). As a result, Ag is distributed within the W-Ti-N matrix in the form of particles. Therefore, all W-Ti-N/Ag films exhibit a fcc structure with three phases coexisting of W_2N, TiN, and Ag.

Based on the above results, we can explain several experimental phenomena that have not been fully explained in this section:

(i) For XRD spectrum, the left-right asymmetry of the deposited diffraction peak is caused by the coexistence of three phases. The three diffraction peaks of the same crystal plane are very close, resulting in the left-right asymmetry of the measured deposited diffraction peak. Compared with nitride ceramics, Ag has a large thermal expansion coefficient [63]. During the cooling process after the deposition of the film, greater thermal stress will be generated. According to the thermal stress calculation formula [64], the thermal stress at this time is tensile type

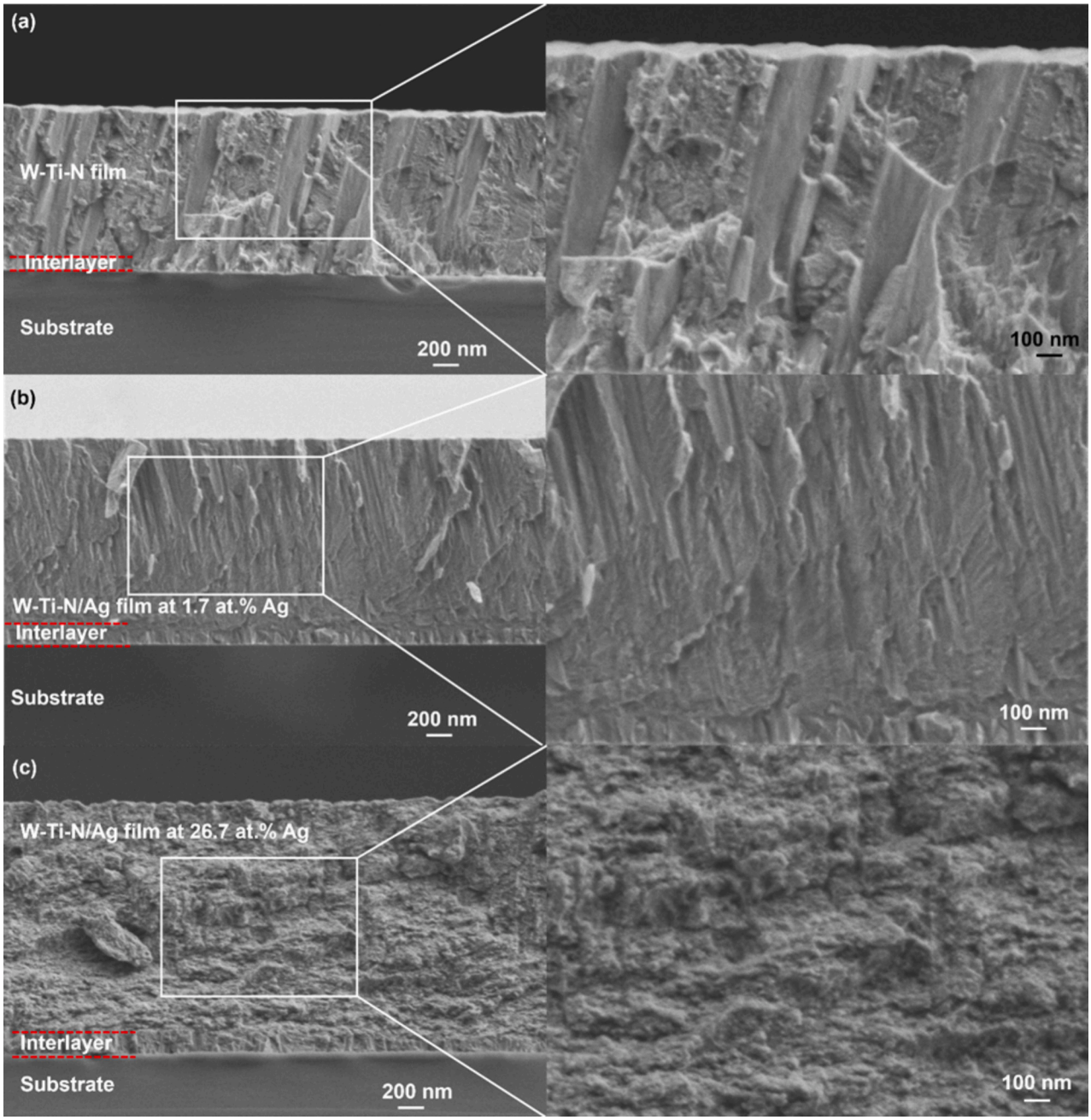

Fig. 4. Cross-sectional SEM images of the W-Ti-N/Ag films with various Ag content: (a) 0 at.% Ag, (b) 1.7 at.% Ag, and (c) 26.7 at.% Ag.

(the calculated value is all positive), which will cause the diffraction peak to shift to higher angles as the Ag content increases. Additionally, the formation of fcc-Ag in the film also contributes to the shoulder at higher angles since standard fcc-Ag XRD peaks are also located at higher angles.

(ii) For the cross-sectional SEM image, Ag is observed as particles distributed within the W-Ti-N matrix, as confirmed by the TEM results. During film growth, these Ag particles hinder the development of the original columnar crystals and act as nucleation sites for new grain formation [64]. Consequently, with the increase of Ag content, the width of the film columnar crystals becomes smaller and smaller, and when the Ag content is high, such as 26.7 at.% Ag, the film completely loses the classic columnar crystal structure of the nitride ceramic matrix. The smooth cross-section of the film is dominated by brittle intergranular fracture, while the rough cross-section is dominated by more plastic transgranular fracture. Due to the incomplete coordination between the grains and the difference in atomic arrangement, higher energy is often accumulated at the grain boundaries [38]. Therefore, under the action of external stress, after the crack initiates, it is easy to expand along the grain boundary direction, resulting in intergranular fracture, and the cross section is relatively smooth. Ag has excellent ductility, and the addition of Ag particles in the W-Ti-N matrix makes the crack extend to the grain boundary and deflect, which hinders the further growth of the crack. As a result, with the addition of Ag, transgranular fracture dominates the fracture of the film cross section. When Ag content is 26.7 at.%, the columnar crystals of the film disappear, and almost no smooth cross section is observed. In addition, as the Ag content increases to 2.7 at.%, the ratio of (W + Ti)/N decreases, and the defects in the lattice increase, which will further prevent the initiation and expansion of microcracks and improve the resistance to plastic deformation.

(iii) Regarding TEM results, it reveals that even at a low Ag content of 1.7 at.%, the Ag particles in the film exhibit relative large sizes, as entire

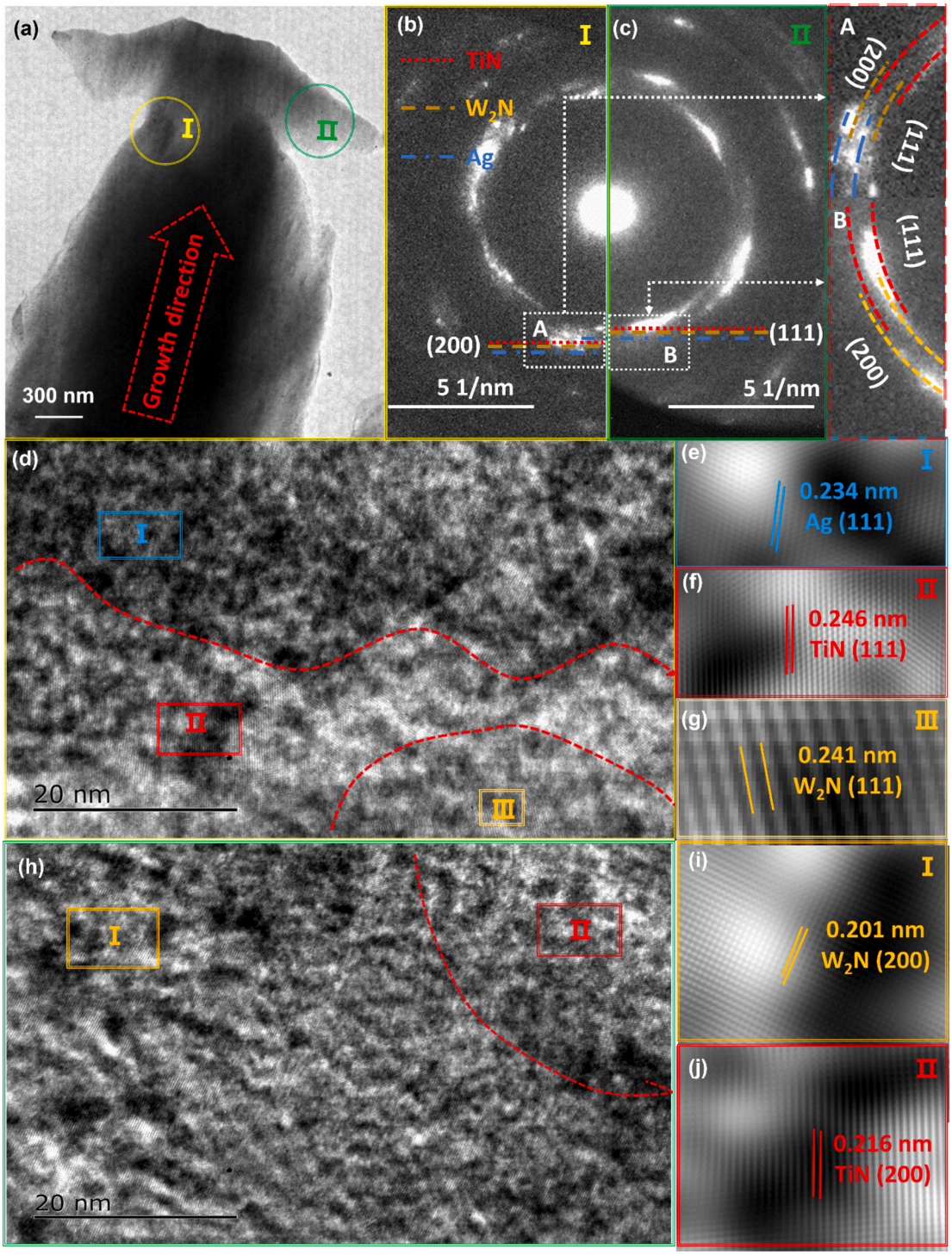

Fig. 5. Cross-sectional TEM image of W-Ti-N/Ag film with Ag content of 1.7 at.% (a), and its SAED spectra in region I (b) and region II (c), HRTEM image in region I in (a) (d) and its corresponding IFFT spectra (e-g), HRTEM image in region II in (a) (h) and its corresponding IFFT spectra (i, j).

particles are not discernible within the HRTEM field of view (Fig. 5d). This finding contrasts with our previous reports where Ag nanoparticles, approximately 8 nm in diameter, were observed in TiN-Ag films containing <5 at.% Ag [38]. Additionally, an epitaxial growth of Ag-SiN_x layer on the Mo_2N template was clearly detected in HRTEM image for its layers smaller than 6 nm [65]. These films were synthesized using a magnetron co-sputtering system, utilizing separate Ti and Ag targets with diameters of 75 mm [66,67]. In contrast, the present study uses a rectangular Ag target to deposit films in a semi-industrial magnetron sputtering system, with the substrate rotating to achieve uniform film coverage. During deposition, even though the Ag target operates at low power, the large surface area of the target results in a substantial amount of Ag being sputtered onto the substrate. Moreover, there is no simultaneous sputtering of W or Ti to inhibit Ag mobility. As a result, Ag atoms freely diffuse across the substrate, leading to aggregation and particle growth. As deposition continues, further growth occurs, resulting in the formation of larger Ag particles.

In summary, the W-Ti-N/Ag film consists of three coexisting phases:

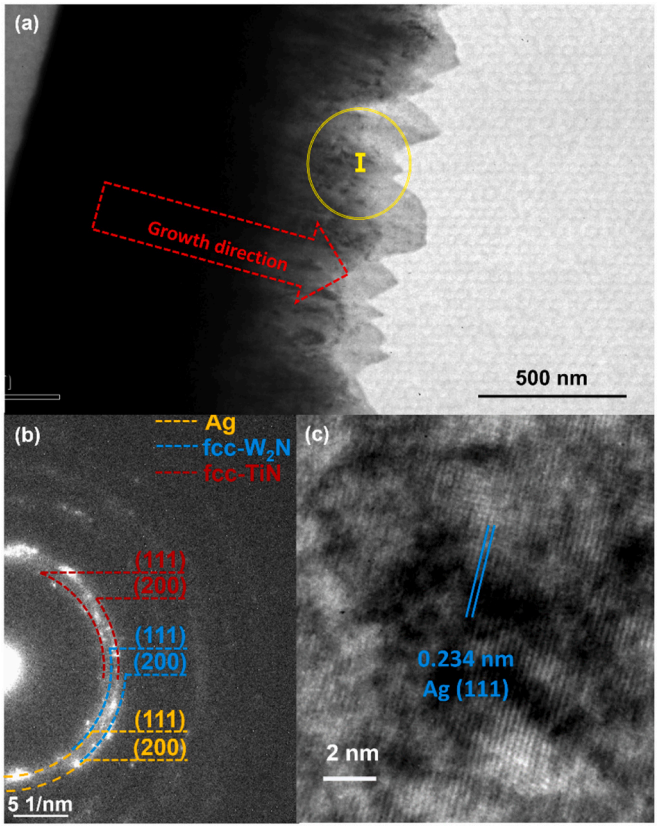

Fig. 6. TEM image of the cross section of W-Ti-N/Ag film with an Ag content of 26.7 at.% (a), SAED at region I (b), and HRTEM image of black particles (c).

fcc-TiN, fcc-W_2N, and fcc—Ag. As the Ag content increases, the film's resistance to plastic deformation improves, while both the number and size of Ag particles increase.

3.2. Mechanical properties

Fig. 7 indicates the hardness and elastic modulus of W-Ti-N/Ag composite films with different Ag contents. As shown in the figure, the hardness and elastic modulus of the W-Ti-N film are 39 and 400 GPa, respectively. Both the hardness and elastic modulus of the W-Ti-N/Ag film gradually decrease with increasing Ag content. When the Ag content exceeds 25 at.%, the hardness and elastic modulus remain relatively stable, averaging around 10 GPa.

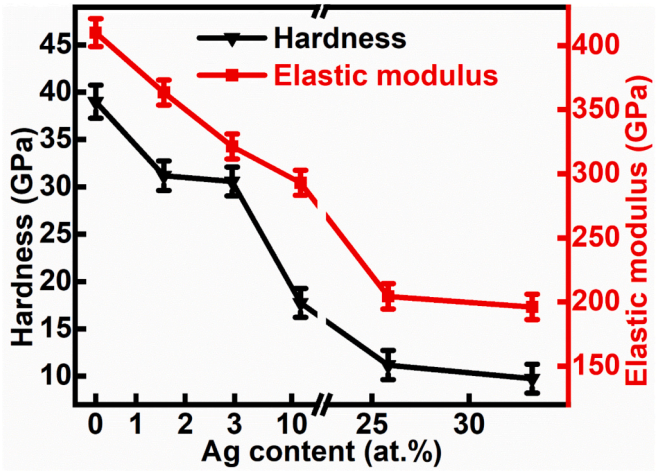

Fig. 7. Hardness and elastic modulus of the W-Ti-N/Ag composite films with various Ag content.

The measured residual stress of the reference W-Ti-N film is in the state of compressive state with a value of approximately −1.9 GPa. However, its value is gradually decreased by the addition of Ag, from about −1.8 GPa for the film with the Ag content of 1.7 at.% to around −0.9 GPa for the film at 32.5 at.% Ag. The residual stress of the as-deposited film is mainly influenced by two factors: the intrinsic stress, and the thermal stress [68]. The addition of Ag could significantly increase the residual thermal stress due to its higher thermal expansion coefficient [69] and, thereby reducing the residual compressive stress of the films.

The main factors affecting the hardness of the W-Ti-N reference film are as follows: (i) Intrinsic hardness of the two phases: W-Ti-N is composed of two phases, W_2N and TiN. According to the elemental composition analysis, W_2N is the main phase. Since the hardness of W_2N (36 GPa [70]) is higher than that of TiN (21 GPa [38]), the overall hardness of the W-Ti-N composite film is primarily determined by the W_2N phase. (ii) Solid solution strengthening: During the deposition process, the solid solution of Ti in the W_2N lattice and the solid solution of W in the TiN lattice cause the lattice distortion of the two phases, resulting in an increase in hardness. (iii) Grain refinement: During the film growth process, the appearance of the TiN phase hinders the growth of the W_2N grains to a certain extent. At the same time, W_2N also prevents the growth of the second phase TiN, resulting in grain refinement in the film [71]. (iv) Residual stress: The as-deposited film's residual stress exhibits a compressive state, and this results in the enhancement on the hardness.

As mentioned above, the addition of Ag leads to the appearance of a third phase fcc-Ag in the film. Although the presence of Ag at the W_2N and TiN grain boundaries during the film growth process can significantly (i) refine the average grain size of the film and (ii) increase the number of interfaces, hindering crack propagation, the extremely low intrinsic hardness of Ag compared to W-Ti-N film causes the overall hardness of the film to gradually decrease with the increase of Ag content (<20 at.% Ag).

The elastic modulus of the film is primarily affected by the strength of the chemical bond. The addition of Ag has minimal impact on the lattice parameters of W_2N and TiN (Ag is difficult to dissolve in the nitride ceramic lattice [72]). Therefore, the extremely low elastic modulus of Ag causes the elastic modulus of the film to gradually decrease with the increase of Ag content.

Ag has been widely used as a lubricant additive in nitride hard films to enhance their self-lubricating properties [39]. Recent studies have further shown that even small amounts of Ag can improve the mechanical properties of these films [73], a result typically attributed to grain refinement caused by the incorporation of Ag [41]. In this paper, the addition of Ag significantly reduces the width of columnar grains, yet the hardness of the film gradually decreases with increasing Ag content. This suggests that while fine grain strengtherning may occur, it is insufficient to counteract the reduction in hardness caused by the inherently low hardness of Ag agent. This finding indicates that the enhancement on mechanical properties observed in nitride ceramic films with low Ag content may be influenced additional mechanisms beyond fine grain strengthening. Our group has previously shown, through the investigation on the Ag-SiN_x/Mo_2N-SiN_x multilayered films, that when the Ag-SiN_x layers is reduced to below 6 nm, they grow coherently with the Mo_2N template [65]. The possibility of the formation of the coherent structure in the nitride-based films containing soft metal was also proved by a case of study of TiN-Ag composite/multilayered films [41]. The results confirmed that the Ag nanoparticles/layers with a size of approximately 4 nm could epitaxially grow with the TiN templates. This coherent growth leads to enhanced mechanical strength, which we identified as the primary factor contributing to the improvement in mechanical properties. In this study, the W-Ti-N/Ag composite films display Ag particle sizes significantly larger than 6 nm at

an Ag content of 1.7 at.%, due to the specific deposition method used. As a result, coherent growth does not occur, which explains the absence of mechanical property enhancement, even at low Ag content. These experimental results further support our earlier conclusion that the enhancement of mechanical properties in ceramic films containing small amounts of soft metals is primarily governed by the size of the soft metal particles, rather than their concentration. This insight offers a new perspective for the future design of such film materials.

4. Conclusion

Alloying hard nitride-based ceramic matrices with soft metal of silver by magnetron sputtering technology is considered one of the most promising strategies for real industrial applications. However, there is limited literature providing actual parameters for industrial-scale PVD methods in the context of such film systems. In this paper, a series of W-Ti-N/Ag composite films was designed and developed using a semi-industrial magnetron sputtering system, and the influence of Ag content on the microstructure and mechanical properties was systemically investigated through SEM/EDS, XRD, XPS, TEM, and nano-indentation analyses.

The results indicated that the reference W-Ti-N film exhibited a dense columnar structure with a dual-phase of fcc-W_2N, and fcc-TiN. The addition of Ag gave rise to a third phase, fcc—Ag, which formed as particles embedded within the crystalline grains of the solid solution of $(WTi)_2N$ and (TiW)N. The dense columnar structure persisted in W-Ti-N/Ag composite films with Ag contents up to 26.7 at.%. However, beyond this level, the columnar structure disappeared, though the film maintained a dense morphology. Grain refinement, increased interface density, and the ductility of Ag contributed to the predominant trans-granular fracture mode observed in the cross-sections of the Ag-doped films. Nevertheless, the expected enhancement on hardness and elastic modulus from Ag, particularly at extremely low content below 5 at.%, was not observed, since the TEM measured size of Ag particles exceeded the critical value for coherent strengthening. As a result, both the hardness and elastic modulus of the composite films gradually decrease with the Ag content due to the soft nature of the Ag phase.

CRediT authorship contribution statement

Jing Luan: Writing – review & editing, Writing – original draft, Methodology, Investigation, Data curation. **Yiping Wang:** Writing - original draft, Investigation, data curation. **Songtao Dong:** Investigation, Data curation. **Manuel Evaristo:** Investigation. **Filipe Fernandes:** Supervision, Funding acquisition, Data curation. **Albano Cavaleiro:** Writing – review & editing, Supervision, Investigation, Funding acquisition, Data curation. **Hongbo Ju:** Writing – review & editing, Writing – original draft, Supervision, Project administration, Methodology, Investigation, Funding acquisition, Data curation, Conceptualization.

Declaration of competing interest

We declare that we do not have any commercial or associative interest that represents a conflict of interest in connection with the work submitted.

Acknowledgements

Supported by the projects granted by the National Natural Science Foundation of China with the number of 52171071 and 51801081, national funds through FCT of Portugal – Fundação para a Ciência e a Tecnologia, under a scientific contract of 2021.04115.CEECIND, 2023.06224.CEECIND, and under projects UID/00285 - Centre for Mechanical Engineering, Materials and Processes and LA/P/0112/2020, the Slovenian Research Agency ARIS under the Research Core Funding Programme of P2-0231 and the Marie Sklodowska-Curie Actions COFUND SCHEME of 5100-237/2023-9.

Data availability

Data will be made available on request.

References

[1] B. Swain, R. Yang-Wallentin, Achieving sustainable development goals: predicaments and strategies, Int. J. Sustain. Dev. World Ecol. 27 (2020) 96–106.
[2] K. Holmberg, A. Erdemir, Influence of tribology on global energy consumption, costs and emissions, Friction 5 (2017) 263–284.
[3] X. Zhang, W. Niu, Y. Dai, H. Xu, J. Dong, Rapid selection of environmentally friendly layered alkaline-earth metal phosphates as solid lubricants using crystallographic data, Sci. Rep. 8 (2018) 16210.
[4] Q. Sun, L. Chen, J. Cheng, S. Zhu, H. Tan, W. Chen, K. Chang, J. Yang, W. Liu, Self-lubrication of single-phase high-entropy ceramic enabled by tribo-induced amorphous carbon, Scr. Mater. 227 (2023) 115273.
[5] O. Hod, E. Meyer, Q. Zheng, M. Urbakh, Structural superlubricity and ultralow friction across the length scales, Nature 563 (2018) 485–492.
[6] W. Liu, Q. Shen, M. Yang, T. Gao, B. Ji, R. Tu, S. Zhang, High hardness and toughness potential TiN/TiSiN gradient nano-multilayer coating structure by finite element study, Ceram. Int. 50 (2024) 9034–9046.
[7] D.G. Subhedar, K.V. Chauhan, D.A. Patel, An experimental investigation of TiN coatings on cutting force and surface finish in milling of aluminum, Materials Today: Proceedings. 59 (2022) 161–165.
[8] C. Thomser, V. Bailescu, S. Brezinsek, J. W. Coenen, H. Greuner, T. Hirai, J. Linke, C. P. Lungu, H. Maier, G. Matthews, Ph. Mertens, R. Neu, V. Philipps, V. Riccardo, M. Rubel, C. Ruset, A. Schmidt, I. Uytdenkhouwen &Contributors Jet Efda. Plasma Facing Materials for the JET ITER-Like Wall. Fusion Science and Technology.*62* (2012): 1–8. doi:10.13182/FST12-A14103.
[9] H.L. Sun, Z.X. Song, D.G. Guo, F. Ma, K.W. Xu, Microstructure and mechanical properties of Nanocrystalline tungsten thin films, J. Mater. Sci. Technol. 26 (2010) 87–92.
[10] Y.G. Shen, Y.W. Mai, D.R. McKenzie, Q.C. Zhang, W.D. McFall, W.E. McBride, Composition, residual stress, and structural properties of thin tungsten nitride films deposited by reactive magnetron sputtering, J. Appl. Phys. 88 (2000) 1380–1388.
[11] M.B. Zellner, J.G. Chen, Surface science and electrochemical studies of WC and W_2C PVD films as potential electrocatalysts, Catal. Today 99 (2005) 299–307.
[12] Q. Zhao, J. Wang, X. Gu, W. Sun, K. Wang, J. Pan, X. Zhu, M. Wen, K. Zhang, Effects of substrate bias voltage on the phase structure, mechanical and wear resistance properties of tungsten boride films, Ceram. Int. 48 (2022) 11535–11544.
[13] K. Affolter, H. Kattelus, M.A. Nicolet, Characterization of W-N alloys formed by sputter deposition, MRS Online Proc. Libr. 47 (1985) 167–173, https://doi.org/10.1557/PROC-47-167.
[14] J. Luan, H. Lu, J. Xu, F. Fernandes, M. Evaristo, B. Ma, F. Xie, A. Cavaleiro, H. Ju, Exploring tribological characteristics of ZrN-MoSN composite films fabricated via RF magnetron sputtering: Insights from microstructure and performance analysis, Surf. Coat. Technol. 484 (2024) 130813.
[15] F.C.T. So, E. Kolawa, X. Zhao, M. Nicolet, WN_x: properties and applications, Thin Solid Films 153 (1987) 507.
[16] H. Ju, F. Kong, J. Xu, Y. Geng, C. Zhang, Influence of Ag on the microstructure, mechanical and tribological properties of SiC-Ag composite film deposited by the industrial DC magnetron sputtering system, Vacuum 218 (2023) 113672.
[17] Y.T. Kim, C.W. Lee, S. Min, New method to improve the adhesion strength of tungsten thin film on silicon by W_2N glue layer, Appl. Phys. Lett. 61 (5) (1992) 537.
[18] T. Nakajima, K. Watanabe, N. Watanabe, Preparation of tungsten nitride film by CVD method using WF_6, J. Electrochem. Soc. 134 (1987) 3175.
[19] O. Wänstrand, M. Larsson, P. Hedenqvist, Mechanical and tribological evaluation of PVD WC/C coatings, Surf. Coat. Technol. 111 (1999) 247–254.
[20] S.S. Grabchikov, O.I. Potuzhnaya, L.B. Sosnovskaya, M.U. Sheleg, Microstructure of amorphous electrodeposited co-Ni-W films, Russian Metallurgy (Metally). 2009 (2009) 164–171.
[21] K. Smyrnova, M. Sahul, M. Haršáni, A. Pogrebnjak, V. Ivashchenko, V. Beresnev, V. Stolbovoy, L. Caplovič, M. Caplovicová, L. Vančo, M. Kusý, A. Kassymbaev, L. Satrapinskyy, D. Flock, Microstructure, mechanical and Tribological properties of advanced layered WN/MeN (me = Zr, Cr, Mo, Nb) nanocomposite coatings, Nanomaterials 12 (2022) 395.
[22] J. Luan, F. Kong, M. Evaristo, F. Fernandes, Y. Zhou, A. Cavalerio, H. Ju, Design and magnetron sputtering of nanomultilayered W_2N/ag-SiN_x films: microstructural insights and optimized self-lubricant properties from room temperature to 500°C, Ceram. Int. 50 (2024) 39226–39234.
[23] D. Javdošňák, J. Musil, Z. Soukup, S. Haviar, R. Čerstvý, J. Houska, Tribological properties and oxidation resistance of tungsten and tungsten nitride films at temperatures up to 500°C, Tribol. Int. 132 (2019) 211–220.
[24] H. Ju, R. Zhou, S. Liu, L. Yu, J. Xu, Enhancement of the tribological behavior of self-lubricating nanocomposite Mo_2N/Cu films by adding the amorphous SiN_x, Surf. Coat. Technol. 423 (2021) 127565.
[25] M. Beltrami, A. Mavric, S.D. Zilio, M. Fanetti, G. Kapun, M. Lazzarino, O. Sbaizero, M. Cekada, A comparative study of nanolaminate CrN/Mo_2N and CrN/W_2N as hard and corrosion resistant coatings, Surf. Coat. Technol. 455 (2023) 129209.
[26] D. Braga, J.P. Dias, A. Cavaleiro, Duplex treatment: W-Ti-N sputtered coatings on pre-nitrided low and high alloy steels, Surf. Coat. Technol. 200 (2006) 4861–4869.

[27] S. Zhang, D. Sun, Y. Fu, H. Du, Effect of sputtering target power on microstructure and mechanical properties of nanocomposite nc-TiN/a-SiNx thin films, Thin Solid Films 447-448 (2004) 462–467.
[28] H. Ju, S. He, L. Yu, I. Asempah, J. Xu, The improvement of oxidation resistance, mechanical and tribological properties of W_2N films by doping silicon, Surf. Coat. Technol. 317 (2017) 158–165.
[29] S. Anwar, A. Islam, S. Bajpai, S. Anwar, Structural and mechanical studies of W_2N embedded Si_3N_4 nanocomposite hard coatings prepared by reactive magnetron sputtering, Surf. Coat. Technol. 311 (2017) 268–273.
[30] L.R. Shaginyan, M. Mišina, J. Zemek, J. Musil, F. Regent, V.F. Britun, Composition, structure, microhardness and residual stress of W-Ti-N films deposited by reactive magnetron sputtering, Thin Solid Films 408 (2002) 136–147.
[31] P. Ren, K. Zhang, X. He, S. Du, X. Yang, T. An, M. Wen, W. Zheng, Toughness enhancement and tribochemistry of the Nb-ag-N films actuated by solute ag, Acta Mater. 137 (2017) 1–11.
[32] W. Gulbiński, T. Suszko, Thin films of Mo_2N/ag nanocomposite—the structure, mechanical and tribological properties, Surf. Coat. Technol. 201 (2006) 1469–1476.
[33] G. Wang, Y. Si, M. Wen, J. Qiu, S. Zhang, Q. Song, W. Wang, X. Yang, P. Ren, Microstructure, mechanical and tribological behaviors of hard-yet-tough Hf-ag-N coating, J. Mater. Res. Technol. 22 (2023) 2030–2042.
[34] H. Li, J. Li, J. Kong, J. Huang, Q. Wu, D. Xiong, Achieving high toughness and wear resistance for hard TaN-ag films actuated by ag, Int. J. Refract. Met. Hard Mater. 111 (2023) 106076.
[35] H. Ju, J. Guo, L. Yu, J. Xu, Enhancement of the mechanical and tribological properties of self-lubricant Mo2N-Ag composite film by adding amorphous SiNx, Ceram. Int. 50 (2024) 8463–8471.
[36] Y. Zhang, Z. Wang, Y. Zhang, X. Bai, S. Zhou, H. Li, Y. Cheng, A. Wang, P. Ke, Self-adaptive lubricating behavior of VAlN/Ag multi-layer coating at simulated operating conditions, J. Mater. Sci. Technol. (2025), https://doi.org/10.1016/j.jmst.2025.01.014.
[37] H. Ju, J. Luan, J. Xu, A. Cavaleiro, M. Evaristo, F. Fernandes, Nano-multilayered ZrN-Ag/Mo-S-N film design for stable anti-frictional performance at a wide range of temperatures, Friction 12 (2024) 2826–2837.
[38] H. Ju, L. Yu, D. Yu, I. Asempah, Microstructure, mechanical and tribological properties of TiN-Ag films deposited by reactive magnetron sputtering, Vacuum 141 (2017) 82–88.
[39] Y. Ren, J. Jia, X. Cao, G. Zhang, Effect of Ag contents on the microstructure and tribological behaviors of NbN-Ag coatings at elevated temperatures, Vacuum 204 (2022) 111330.
[40] P. Ren, S. Zhang, J. Qiu, X. Yang, W. Wang, Y. Li, Y. Si, G. Wang, M. Wen, Self-lubricating behavior of VN coating catalyzed by solute Ag atom under dry friction and oil lubrication, Surf. Coat. Technol. 409 (2021) 126845.
[41] J. Luan, F. Kong, J. Xu, F. Fernandes, M. Evaristo, S. Dong, A. Cavaleiro, H. Ju, Deciphering the mechanical strengthening mechanism: Soft metal doping in ceramic matrices-A case study of TiN-Ag films, Mater. Des. 248 (2024) 113489.
[42] X.C. Zhang, B.S. Xu, H.D. Wang, Y.X. Wu, Optimum designs for multi-layered film structures based on the knowledge on residual stresses, Applied Surface Science. Applied Surface Science. 253 (2007) 5529–5535.
[43] P.N. Silva, J.P. Dias, A. Cavaleiro, Tribological behaviour of W-Ti-N sputtered thin films, Surf. Coat. Technol. 200 (2005) 186–191.
[44] J.C. Oliveira, A. Cavaleiro, C.M.A. Brett, Influence of sputtering conditions on corrosion of sputtered W-Ti-N thin film hard coatings: salt spray tests and image analysis, Corros. Sci. 42 (2000) 1881–1895.
[45] V.A. Alves, C.M.A. Brett, A. Cavaleiro, Electrochemical corrosion of magnetron sputtered WTiN-coated mild steels in a chloride medium, Surf. Coat. Technol. 161 (2002) 257–266.
[46] G. Greczynski, L. Hultman, X-ray photoelectron spectroscopy: towards reliable binding energy referencing, Process in Material Science. 107 (2020) 100591.
[47] S.A.A. Terohid, S. Heidari, A. Jafari, S. Asgary, Effect of growth time on structural, morphological and electrical properties of tungsten oxide nanowire, Applied Physics A 567 (2018).
[48] H. Zhao, C. Mu, F. Ye, The effect of modulation of period on the mechanical and wear properties of TiAgN/W_2N coatings, Surf. Coat. Technol. 309 (2017) 29–34.
[49] D. Li, K. Gao, Z. Miao, Y. Miao, X. Wang, D. Wang, Z. Li, Y. Han, Q. Zheng, Z. Li, C. Sun, Localized nitride strategy to construct interfacial and electronic modulated WO_3/WN nanoparticles for superior lithium-ion storage, J. Colloid Interface Sci. 677 (2025) 1034–1044.
[50] S. Oktay, Z. Kahraman, M. Urgen, K. Kazmanli, XPS investigations of tribolayers fomed on TiN and (Ti, re) N coatings, Appl. Surf. Sci. 328 (2015) 255–261.
[51] A.M. Kia, J. Speulmanns, S. Bonhardt, J. Emara, K. Kuhnel, N. Haufe, W. Weinreich, Spectroscopic analysis of ultra-thin TiN as a diffusion barrier for lithium-ion batteries by ToF-SIMS, XPS, and EELS, Appl. Surf. Sci. 564 (2021) 150457.
[52] S. Lu, J. Ding, X. Wei, K. Lee, Z. Chen, W. Yang, J. Qiao, K. Chen, D. Zhang, W. Zhang, X. Li, Structural modulation and frictional, antibacterial and biocompatible properties of ag-incorporated DLC films: dependence on ag precipitation behavior, Appl. Surf. Sci. 677 (2024) 161078.
[53] D. He, L. Cao, J. Huang, S. Li, Y. Feng, G. Li, F. Wang, L. Feng, Synergistic coupling of heterogeneous VN/WN nanoparticles embedded in N-doped carbon matrix for efficient hydrogen evolution reaction, Chem. Eng. J. 429 (2022) 131945.
[54] Q. Zhang, Q. Chen, T. Su, Z. Li, Q. Zhao, C. Ju, G. Zhao, F. Guo, X. Wang, Study on the tribological behavior of TiN-VN/PAO composite lubricant system: ZIF-8 as a lubricating additive, Tribol. Int. 200 (2024) 110128.
[55] S. Rtimi, C. Pulgarin, M. Bensimon, J. Kiwi, Evidence for TiON sputtered surfaces showing accelerated antibacterial activity under simulated solar irradiation, Sol. Energy 93 (2013) 55–62.
[56] D. Li, K. Gao, Z. Miao, Y. Miao, X. Wang, D. Wang, Z. Li, Y. Han, Q. Zheng, Z. Li, C. Sun, Localized nitride strategy to construct interfacial and electronic modulated WO_3/WN nanoparticles for superior lithium-ion storage, J. Colloid Interface Sci. 677 (2025) 1034–1044.
[57] S. Vargas-Villanueva, D.A. Torres-Ceron, S. Amaya-Roncancio, I.D. Arellano-Ramirez, J.S. Riva, E. Restrepo-Parra, Study of the incorporation of S in TiO_2/SO_4^{2-} coatings produced by PEO process through XPS and DFT, Appl. Surf. Sci. 599 (2022) 153811.
[58] H. Jeon, J.H. Park, S. Han, S.H. Ahn, J. Baik, H. Lee, H.S. Ahn, S. Hong, W-O bond shortening by doping of first-row transition metal ions that enhances its catalytic potency, Appl. Surf. Sci. 567 (2021) 150834.
[59] L. Wang, Y. Zhang, P. Guo, R. Chen, P. Ke, Z. Wang, A. Wang. Designing sandwich-zigzag multilayered TiN coatings for corrosion-erosion coupling damage protection. Ceram. Int. doi:https://doi.org/10.1016/j.ceramint.2024.08.306.
[60] F. Yan, B. Jiang, Z. Wang, Thermal stabilization of nanocrystalline promoting conductive corrosion resistance of TiN-ag films for metal bipolar plates, Vacuum 195 (2022) 110631.
[61] H. Ju, N. Ding, J. Xu, L. Yu, I. Asempah, J. Xu, G. Yi, B. Ma, Crystal structure and the improvement of the mechanical and tribological properties of tungsten nitride films by addition of titanium, Surf. Coat. Technol. 345 (2018) 132–139.
[62] R. Zhou, H. Ju, S. Liu, Z. Tong, J. Xu, L. Yu, H. Qian, S. Jia, R. Song, J. Shen, The influences of ag content on the friction and wear properties of TiCN-ag films, Vacuum 196 (2022) 110719.
[63] X. Zhou, B. Huang, T. Zhang, Size and temperature-dependent Young's modulus and size-dependent thermal expansion coefficient of thin films, Phys. Chem. Chem. Phys. 18 (2016) 21508.
[64] X. Zhu, Z. Xiao, J. An, H. Jiang, Y. Jiang, Z. Li, Microstructure and properties of cu-ag alloy prepared by continuously directional solidification, J. Alloys Compd. 883 (2021) 160769.
[65] H. Ju, J. Luan, Y. Wang, A. Bondarev, M. Evaristob, Y. Geng, J. Xu, A. Cavaleiro, F. Fernandes, Mutual promotion on the mechanical and tribological properties of the nacre-like self-lubricant film designed for demanding green tribological applications, Friction 13 (3) (2025) 9440963, https://doi.org/10.26599/FRICT.2025.9440963.
[66] H. Ju, L. Yu, S. He, I. Asempah, J. Xu, Y. Hou, The enhancement of fracture toughness and tribological properties of the titanium nitride films by doping yttrium, Surf. Coat. Technol. 321 (2017) 57–63.
[67] H. Ju, L. Xu, J. Luan, Y. Geng, J. Xu, L. Yu, J. Yang, F. Fernandes, Enhancement on the hardness and oxidation resistance property of TiN/ag composite films for high temperature applications by addition of Si, Vacuum 209 (2023) 111752.
[68] M. Huff, Review paper: residual stresses in deposited thin-film material layers for Micro- and Nano-Systems manufacturing, Micromachines 13 (2022) 2084.
[69] S. Ochiai, H. Rokkaku, J.K. Shin, S. Iwamoto, H. Okuda, K. Osamura, M. Sato, A. Otto, A. Malozemoff, Thermally and mechanically induced residual strain and strain tolerance of critical current in stainless steel-laminated Bi2223/ag/ag alloy composite superconductors, Supercond. Sci. Technol. 21 (2008) 075009.
[70] A. Salamat, A.L. Hector, P. Kroll, P.F. McMillan, Nitrogen-rich transition metal nitrides, Coord. Chem. Rev. 257 (2013) 2063–2072.
[71] W. Liu, Y. Wang, X. Cao, X. Liu, B. Sun, H. Wang, X. Yi, X. Meng, Z. Gao, Synergistic effect of TiN ceramic particle and grain refinement in enhancing the higher performance Ti-V-Al based shape memory alloy, J. Mater. Res. Technol. 29 (2024) 5633–5645.
[72] S.C. Velasco, A. Cavaleiro, S. Carvalho, Functional properties of ceramic-ag nanocomposite coatings produced by magnetron sputtering, Prog. Mater. Sci. 84 (2016) 158–191.
[73] G. LiuK. WangY. PanD. YangX. YuZ. NieJ. ZhuJ. HanC. TanEffect of ag content and extrusion on the microstructure and mechanical properties of mg-ag alloysJ. Mater. Res. Technol.30202459165926.